Front. Optoelectron. 2012, 5(3): 317–321
DOI 10.1007/s12200-012-0266-x

RESEARCH ARTICLE

Transfer matrix modeling of avalanche photodiode

Saeed OLYAEE (✉)[1], Mohammad SOROOSH[2], Mahdieh IZADPANAH[1]

1 Nano-Photonics and Optoelectronics Research Laboratory, Faculty of Electrical and Computer Engineering, Shahid Rajaee Teacher Training University (SRTTU), Lavizan 16788, Iran
2 Engineering Faculty, Shahid Chamran University, Ahvaz 61355-158, Iran

Abstract In this article, we calculated and modeled the gain of $In_{0.53}Ga_{0.47}As/InP$ avalanche photodiode (APD) based on a device mechanism and carrier rate equations using transfer matrix method (TMM). In fact, a distributed model was presented for calculating impact ionization (I^2) and relating different sections of the multiplication region. In this proposed model, recessive equations were used, and device gain is considered proportional to the number of output photo-electrons and photo-holes. By comparison of simulated results with experimental data available in literature, it has been demonstrated the capability of the developed model as a powerful tool for simulating APDs' behavior and interpreting their experimentally measured characteristics.

Keywords avalanche photodetector (APD), impact ionization (I^2), transfer matrix method (TMM)

1 Introduction

The photodetectors are one of the most important devices in fiber optic and free space optical telecommunication. Generally, they are the first elements in optical receiver that convert optical data to electrical signal. Because of impact ionization (I^2) mechanism in the avalanche photodiode (APD), this device has current gain that plays the role of detecting and amplifying, and hence it has been attracted so much attention among other detectors. In addition, generally, there is no need of external circuits of amplifiers due to current gain. I^2 mechanism is a very important occurring in a multiplication region repetitively. So, to analyze APD, I^2 phenomenon must be firstly simulated, and then other important mechanisms, such as drift, scattering, and absorption process, should be also considered.

Received April 30, 2012; accepted June 5, 2012

E-mail: s_olyaee@srttu.edu

There are different methods for simulation of I^2 mechanisms in semiconductor devices. Here, the recent developments in simulation and modeling of avalanche photodetectors are categorized in analytic, modeling and numerical methods. Analytic approaches are led to final equations to describe device characteristics directly. In 2010, an analytic approach was introduced, in which the effects of optical phonon scattering loss on the characteristics of APD had been studied with multiplication regions as narrow as 25 nm [1].

Circuit modeling is another conventional method converting device equations to their equivalent circuit models. In 1996, a circuit model of PIN APDs was presented based on carrier rate equations [2]. A circuit modeling of separate absorption, charge and multiplication APD was developed in 2003, that device noise has been simulated in addition to APD's characteristics description [3]. A novel equivalent circuit for separate absorption grading charge multiplication APDs composed of basic circuit components was reported in 2010 [4]. Also, the co-simulation of a packaged APD trans-impedance amplifier-module was carried out.

Another new model has been developed, which simulates a real Geiger–APD using VHDL-AMS codes [5]. A staircase approximation of the non-uniform field in the multiplication region and its surrounding was deployed to model thin APD in 2010 [6]. The third approaches of simulation of devices mechanism are numerical models possessing good accurate. An experimental and numerical analysis had been carried out to investigate the impact of picosecond laser pulse waveform on detection efficiency of gated-mode APD for single photon detection in 2010 [7].

The non-equilibrium carrier distribution in an InGaAs/InP APD under light illumination is studied by cross-sectional scanning capacitance microscopy combined with numerical simulation [8]. In 2010, a model was presented to calculate gain and excess noise factor by Monte Carlo method [9]. A full-band Monte Carlo model has been reported to understand the carrier multiplication process in

HgCdTe infrared APDs [10].

A numerical method, for the first time to the best of our knowledge, was presented here to model the multiplication region section-to-section. In fact, transfer matrix method (TMM) is used to relate different sections of multiplication region and insert output carriers of one section to the later section.

The rest of the paper is categorized as follows: in the next section, APD modeling is presented by the TMM. In Section 3, the simulation results of APD modeling are described and investigated. Finally, conclusions are drawn from this investigation in Section 4.

2 APD modeling by TMM

Considering illumination through n side (ITNS), the following carrier's rate equations can be used for reversed biased PIN structure [2]:

$$\frac{\mathrm{d}N_i}{\mathrm{d}t} = N_{G_i} + \upsilon_n\zeta_n N_i + \upsilon_p\zeta_p P_i - \frac{N_i}{\tau_{nt}} - \frac{N_i}{\tau_{nr}} + \frac{I_n}{q}, \quad (1)$$

$$\frac{\mathrm{d}P_i}{\mathrm{d}t} = P_{G_i} + \upsilon_n\zeta_n N_i + \upsilon_p\zeta_p P_i - \frac{P_i}{\tau_{pr}} - \frac{P_i}{\tau_{pt}} + \frac{I_p}{q}, \quad (2)$$

where N_i and P_i are the total excess electrons and holes in the i region, $N_{G_i} = P_{G_i}$ is the generation rate in i region, υ_n and υ_p are the drift velocities of electron and hole in i region, and ζ_n and ζ_p are the I^2 rates of electron and hole in i region. Here, τ_{nr} and τ_{pr} are the recombination life time of electron and hole in i region, and τ_{nt} and τ_{pt} are the transit time of electron and hole through i region. And finally, the hole and electron diffusion current in n and p regions are respectively denoted by I_p and I_n, and the electron charge is denoted by q.

Also, the generation rate in i region is [2]:

$$N_{G_i} = \frac{P_{\mathrm{in}}(1-R)\exp(-\alpha_n W_n)}{h\nu}[1-\exp(-\alpha_i W_i)], \quad (3)$$

where R is the facet reflectivity of n region and $h\nu$ is the photon energy. The absorption coefficient and the width of each section are respectively denoted by α and W.

According to the rate equations and TMM, $In_{0.53}Ga_{0.47}As/InP$ PIN-APD parameters are simulated in MATLAB. The schematic structure of a multiplication region is shown in Fig. 1. In this figure, n and h are represented for photo-electrons and photo-holes with vice versa orientations to each other. For Applying the numerical TMM, multiplication region is divided to M-sections with the length of $\Delta z = W_i/M$ for each.

It should be mentioned that electrons and holes have different coefficients in each section and according to their orientations; the total photo-current is sum of the carrier's left multiplication region from both sides. This can be achieved by multiplying matrixes of all sections in TMM. According above and Fig. 2, one can write

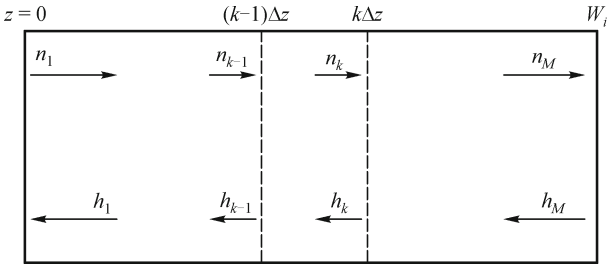

Fig. 1 TMM in analyzing PIN-APD

$$n_k = An_{k-1} + Bh_{k+1}, \quad (4)$$

$$h_k = Cn_{k+1} + Dh_{k-1}. \quad (5)$$

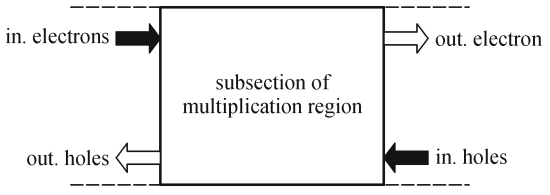

Fig. 2 Schematic drawing of entrance and exit of carriers in subsection of multiplication region

Since, the transfer matrix is obtained from multiplying all layers matrixes, a loop can be written for each subsection in MATLAB. In other words, the total transfer matrix is as follows:

$$\boldsymbol{T} = \begin{bmatrix} A & B \\ C & D \end{bmatrix} = \boldsymbol{T}_1\boldsymbol{T}_2\boldsymbol{T}_3\ldots\boldsymbol{T}_k\ldots\boldsymbol{T}_M. \quad (6)$$

So, the relation between input and output carriers would be [11]

$$\begin{bmatrix} n_M \\ h_M \end{bmatrix} = \boldsymbol{T}\begin{bmatrix} n_1 \\ h_1 \end{bmatrix}. \quad (7)$$

And for drift current, we have

$$I_{\mathrm{Drift}} = [n_{\mathrm{total}} + h_{\mathrm{total}}]q/\mathrm{d}t, \quad (8)$$

where n_{total} and h_{total} are total photo-electrons and photo-holes, q is the electric charge and $\mathrm{d}t$ is time interval. The current through APD is

$$I_{\mathrm{J}} = I_{\mathrm{Drift}} + I_{\mathrm{Diffusion}}. \quad (9)$$

The first term is the drift current and the second is the diffusion current calculated in Ref. [2].

3 Simulation results

According to the parameters in Refs. [6,12,13] and running the programs in MATLAB, the results are shown here. First, the photocurrent is simulated as a function of reverse bias for three different incident light powers (Fig. 3). The simulation result obtained by TMM is in good agreement with the result reported in Ref. [2], as shown in Fig. 3. Considering constant multiplication region, by increasing bias voltage, electric field also augments, and consequently avalanche rate and photocurrent become higher.

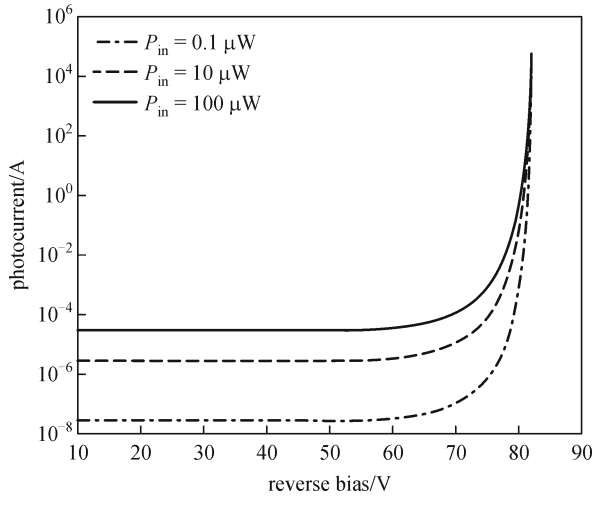

Fig. 3 Photocurrent as function of reverse bias obtained by TMM

Figure 4 shows photocurrent versus reverse bias for three different multiplication regions. With the increasings W_i and reverse bias, depletion region becomes bigger and avalanche breakdown occurs in higher voltages and consequently photocurrent decreases. Considering constant W_i, when reverse bias increases, electric field and hence photocurrent increase. Figure 5 shows the quantum efficiency versus reverse bias. The results represented a good adjustment between the present model and circuit model in Ref. [2] and demonstrated the capability of the TMM model.

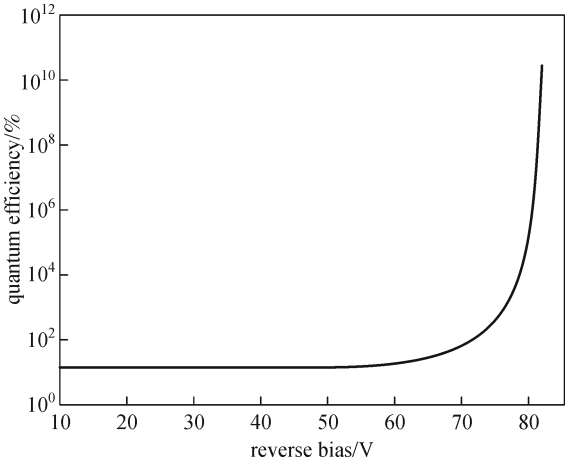

Fig. 5 Quantum efficiency as function of reverse bias obtained by TMM

In Fig. 6, photocurrent and dark current are simulated for $P_{in} = 100$ μW. The dark current is proportional to gain [1] and by increasing reverse bias close to breakdown voltage it has an exponential augmentation. The gain graph as a function of reverse bias is shown in Fig. 7. As shown, with the advance of reverse bias, the intensity of electric field also increases and then gain increases. By increasing multiplication region at a constant bias voltage, the electric field decreases and gain decreases, too. So, to achieve more gain with increasing wavelength, the reverse bias has better been increased.

Figure 8 shows excess noise factor versus gain for $W_i = 2.5$ μm and $W_i = 4.2$ μm. Excess noise factor is the

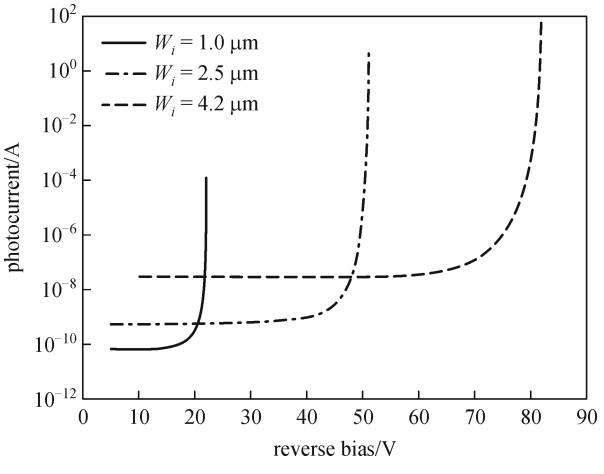

Fig. 4 Photocurrent versus reverse bias for different multiplication region and P_{in} = 100 μW

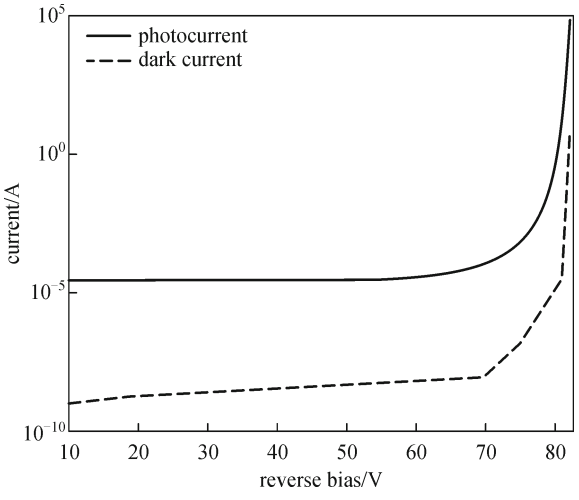

Fig. 6 Current as function of reverse bias (P_{in} = 100 μW)

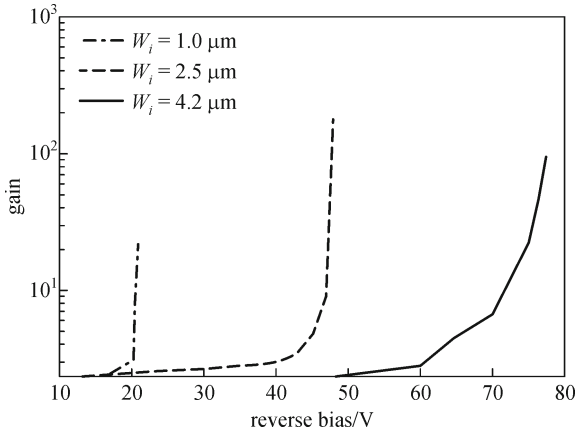

Fig. 7 Gain versus reverse bias (P_{in} = 100 μW)

average of the square of M_i to the square of the gain average [14]:

$$F = \frac{<M_i^2>}{M^2}, \tag{10}$$

where M_i is the gain corresponding to the i-section in multiplication region and gain average, M is multiplication factor.

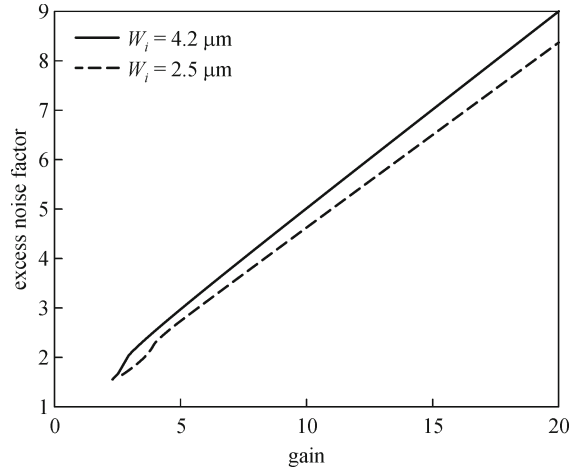

Fig. 8 Excess noise versus gain (P_{in} = 100 μW) for W_i = 2.5 and 4.2 μm

Assuming constant multiplication region, increasing gain enhances excess noise factor. In fact increasing gain means the average growth of the number of impact ionization phenomena and hence ionization length scattering. Considering constant gain, increasing the multiplication region width means increasing average of the ionization length (or decreasing the electric field). This causes the enhancements of carrier scattering and excess noise factor. I^2 number, scattering and excess noise factor increase. In the other hands, when the gain is constant, the increasing of multiplication region raises average of I^2 length, carriers scattering, and eventually excess noise factor.

Figure 9 shows shot noise as a function of reverse bias voltage for three incident optical powers. In constant reverse bias, shot noise increases with optical power due to the augment of photocurrent, that is to say, shot noise depends on photocurrent. Also, since more photons illuminate for the detector, the accidental photon absorption and shot noise increase.

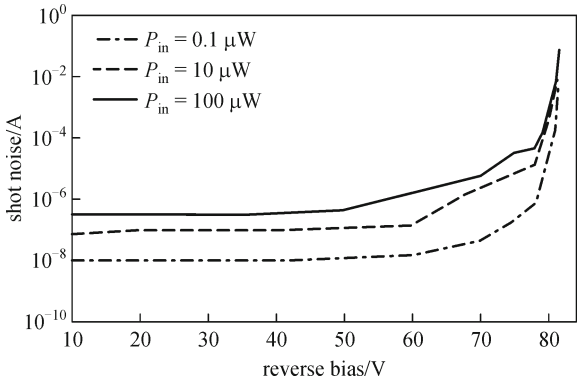

Fig. 9 Shot noise versus reverse bias for different incident light powers

Considering constant optical power, increasing of shot noise resulting from bias voltage raising. This can be paraphrased that because electric field becomes more intense in multiplication region, I^2 of noise carriers increases.

4 Conclusions

In this paper, a PIN-APD was simulated by TMM that estimates device gain with good approximation. In the proposed model, a distributed matrix model was presented by determining rate equations and converting to their matrix equivalents. As a matter of fact, TMM can be used to simulate APD's behavior efficiently and present a microscopic image of carrier's movement. The results in this study are in good agreement with the results of Ref. [2] and experimental data in Ref. [15].

References

1. Masudy-Panah S, Moravvej-Farshi M K. An analytic approach to study the effects of optical phonon scattering loss on the characteristics of avalanche photodiodes. IEEE Journal of Quantum Electronics, 2010, 46(4): 533–540
2. Chen W Y, Liu S Y. PIN avalanche photodiode model for circuit simulation. IEEE Journal of Quantum Electronics, 1996, 32(12): 2105–2111
3. Zarifkar A, Soroosh M. Circuit modeling of separate absorption,

charge and multiplication avalanche photodiode (SACM-APD). In: Proceedings of IEEE the 6th International Conference on Laser and Fiber-Optical Networks Modeling (LFNM). 2004, 213–219

4. Wu J Y, Wang G. A novel equivalent circuit model for separate-absorption-grading-charge multiplication avalanche photodiode (APD) based optical receiver. Journal of Lightwave Technology, 2010, 28(5): 784–790
5. Jradi K, Pellion D, Esteve D, Boizard J L, Le Padellec A, Bazer-Bachi A R. Computer aided design (CAD) model for silicon avalanche Geiger mode systems design: Application to high sensitivity imaging systems. Nuclear Instruments and Methods in Physics Research A, 2010, 626–627(11–12): 77–81
6. Jalali M, Moravvej-Farshi M K, Masudy-Panah S, Nabavi A. An equivalent lumped circuit model for thin avalanche photodiodes with nonuniform electric field profile. Journal of Lightwave Technology, 2010, 28(23): 3395–3492
7. Fang J B, Liao C J; Jiang Z L, Wei Z J, Wang J D, Liu S H. Impact of picosecond laser pulse waveform on detection efficiency of gated-mode avalanche photodiodes for quantum key distribution. Optics Communications, 2010, 284(3): 833–837
8. Yin H, Li T X, Hu W D, Wang W J, Li N, Chen X S, Lu W. Nonequilibrium carrier distribution in semiconductor photodetectors: surface leakage channel under illumination. Applied Physics Letters, 2010, 96(26): 263508
9. Soroosh M, Moravvej-Farshi M K, Saghafi K. A simple empirical model for calculating gain and excess noise in GaAs/AlGaAs APDs. IEICE Electronics Express, 2008, 5(20): 853–859
10. Bertazzi F, Michele M, Penna M, Goano M, Bellotti E. Full-band Monte Carlo simulation of HgCdTe APDs. Journal of Electronic Materials, 2010, 39(7): 912–917
11. Ghafouri-Shiraz H. The Principle of Semiconductor Laser Diodes and Amplifier: Analysis and Transmission Line Laser Modeling. London: Imperial College Press, 2004
12. Kim D S, Lee S Y, Lee J H, Oh G S, Kim N J, Lee J W, Kim A S, Sin Y K. Fabrication of planar InP/InGaAs avalanche photodiode without guard rings. In: Proceedings of IEEE Lasers and Electro-Optics Society Annual Meeting (LEOS 96). 1996, 332–333
13. Tan L J J, Ng J S, Tan C H, David J P R. Avalanche noise characteristics in submicron InP diodes. IEEE Journal of Quantum Electronics, 2008, 44(4): 378–382
14. Kwon O H, Hayat M M, Wang S, Campbell J C, Holmes A, Pan Y, Saleh B E A, Teich M C. Optimal excess noise reduction in thin heterojunction $Al_{0.6}Ga_{0.4}As$-GaAs avalanche photodiodes. IEEE Journal of Quantum Electronics, 2003, 39(10): 1287–1296
15. Anselm K A, Nie H, Hu C, Lenox C, Yuan P, Kinsey G, Campbell J C, Streetman B G. Performance of thin separate absorption, charge, and multiplication avalanche photodiode. IEEE Journal of Quantum Electronics, 1998, 34(3): 482–490